Available online at www.sciencedirect.com
ScienceDirect
Surface Science 602 (2008) 1299–1305
SURFACE SCIENCE
www.elsevier.com/locate/susc

A combined DFT/LEED-approach for complex oxide surface structure determination: $Fe_3O_4(001)$

R. Pentcheva [a,*], W. Moritz [a], J. Rundgren [b], S. Frank [c], D. Schrupp [c], M. Scheffler [d]

[a] Department of Earth and Environmental Sciences, University of Munich, Theresienstrasse 41, 80333 Munich, Germany
[b] Department of Theoretical Physics, Royal Institute of Technology (KTH), SE-10691 Stockholm, Sweden
[c] Department of Physics, University of Augsburg, Germany
[d] Fritz-Haber-Institut der Max-Planck-Gesellschaft, Faradayweg 4-6, D-14195 Berlin, Germany

Received 16 October 2007; accepted for publication 8 January 2008
Available online 15 January 2008

Abstract

A combination of density functional theory (DFT) calculations and low energy electron diffraction (LEED) analysis is used to determine the surface structure of Fe_3O_4 (100). We find that the surface is rich in oxygen and the observed $(\sqrt{2}\times\sqrt{2})R45^\circ$ reconstruction is a result of a Jahn–Teller distortion as established by recent DFT-calculations [R. Pentcheva, F. Wendler, H.L. Meyerheim, W. Moritz, N. Jedrecy, M. Scheffler, Phys. Rev. Lett. 94 (2005) 126101]. The corresponding Pendry reliability factor is 0.34. Furthermore, we investigate the influence of the preparation conditions (temperature, oxygen pressure) on the LEED intensities of natural and synthetic samples. The electron scattering phase shifts used in the analysis of the LEED spectra are derived from two methods, one based on the DFT electron densities and another employing an overlap of atomic potentials with optimized muffin-tin radii. Both approaches lead to similar results.

Keywords: Iron oxide; Magnetite; Fe_3O_4 (001); Low index single crystal surfaces; Surface reconstruction and relaxation; Magnetic surfaces; Density functional theory (DFT); Low energy electron diffraction (LEED)

1. Introduction

The surface properties of transition metal oxides, like chemical activity, magnetism, and conductivity, depend sensitively on the surface geometry and stoichiometry. Knowledge of the surface structure is therefore essential to understand electronic phenomena at oxide surfaces. However, the structural determination is often a challenge to low energy electron diffraction (LEED) and other techniques for quantitative analysis of surfaces because it involves a large number of atoms, resulting often in 50–100 degrees of freedom. A viable procedure to resolve the surface structure is to combine diffraction analysis with density functional theory (DFT) calculations. The latter provide not only structural information but also means for comparing the stability of different configurations. In this paper we apply this approach to determine the surface structure of Fe_3O_4 (001).

Recent explorations of spintronics materials have stimulated new interest in magnetite, due to a predicted half-metallic behavior [1,2] together with a high Curie temperature of 858 K. Magnetite has the inverse spinel structure $Fe^{3+}(Fe^{3+}, Fe^{2+})O_4$ where Fe^{3+} cations occupy a quarter of the tetrahedral A sites and Fe^{3+} and Fe^{2+} ions occupy half of the octahedral B sites. In the [001] direction two types of layers alternate, containing either tetrahedral iron (A layer) or oxygen and octahedral iron (B layer). Consequently, there are two possible volume truncations, shown in Fig. 1. In an ionic picture these two terminations are polar with a nonvanishing dipole moment of the building unit perpendicular to the surface. According to electrostatic considerations in the scheme of Tasker [3] such terminations should have a diverging surface energy and

* Corresponding author. Tel.: +49 89 2180 4352.
E-mail address: pentcheva@lrz.uni-muenchen.de (R. Pentcheva).

0039-6028/$ - see front matter © 2008 Elsevier B.V. All rights reserved.
doi:10.1016/j.susc.2008.01.006

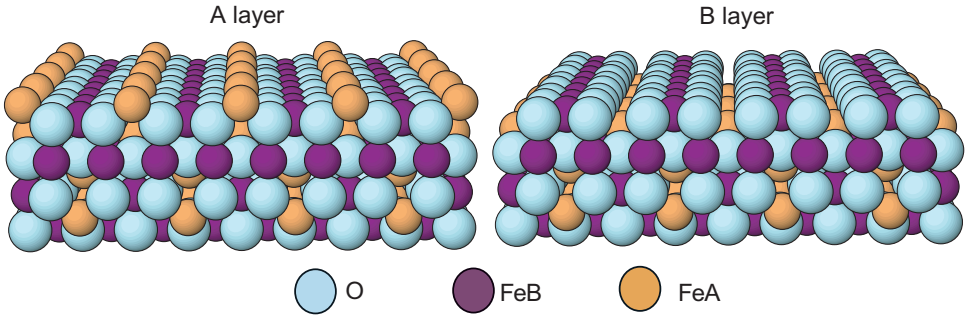

Fig. 1. Possible bulk truncations of $Fe_3O_4(001)$, either with an A layer of tetrahedral iron (left), or a B layer (right panel) containing octahedral iron and oxygen. Oxygen, Fe_A and Fe_B ions are marked with cyan (light grey), orange (grey) and pink (dark grey) circles, respectively. (For interpretation of the references in color in this figure legend, the reader is referred to the web version of this article.)

therefore were often ruled out in previous studies of the surface termination of $Fe_3O_4(001)$. For polar surfaces both the ionic model of Tasker and the autocompensation rule [4] (analogous to the electron counting rule for semiconductor surfaces) predict reconstructions or faceting. Indeed, a $(\sqrt{2}\times\sqrt{2})R45^\circ$-pattern has been measured experimentally [6,5,7–9,11], but the atomic structure has been subject of a long controversy in the literature. A variety of models designed to fulfill the autocompensation rule were proposed to explain the observed periodicity. The most common are the A-layer where every second tetrahedral iron is missing (cf. Fig. 2a) [6–8,10] and the B-termination with an oxygen vacancy (cf. Fig. 2b) [9,11]. Also, a termination with a B-layer and the formation of a surface bipolaron [12,13] as well as a full A-layer where iron ions form dimers have been discussed [14]. To resolve this long standing debate, we have recently performed a full structural optimization of the models proposed in the literature as well as of the two bulk truncations based on DFT calculations and an X-ray diffraction (XRD) analysis and found that the simple ionic picture is not applicable to magnetite [15]. The surface phase diagram constructed in the framework of *ab initio* thermodynamics [16,17] revealed that a modified B-layer is stabilized over a broad range of oxygen pressures. Instead of an ordering of surface defects as in previously proposed models, the symmetry lowering is realized by a wave-like Jahn–Teller distortion. A XRD analysis [15] and scanning tunneling microscopy (STM) measurements [11,18] are consistent with the DFT-model. We note that also the surface bipolaron model proposed by Shvets and collaborators [13] is closely related to the modified B-termination.

In this paper we complement our study by low energy electron diffraction (LEED) measurements and a combined DFT- quantitative LEED $I(V)$ structural analysis. In Section 2 we compare the LEED $I(V)$-curves of natural and synthetic samples and investigate the influence of the oxygen partial pressure and the annealing temperature on the LEED intensity curves. We also discuss the subtleties of a LEED analysis of a complex oxide structure. In particular, we investigate two different ways for generating electron scattering phase shifts for an ionic compound. Phase shifts obtained from DFT calculations both for bulk and surface slab structures are compared with phase shifts based on superpositions of atomic electron densities [19]. Starting from the geometries obtained from DFT [15], several LEED and DFT-optimization cycles with different start geometries have been performed to avoid local minima in the optimisation and to ensure quantitative agreement between the different methods. This combination of DFT-, LEED- and XRD-refinement (the latter presented in Ref. [15]) turns out to be essential for a reliable struc-

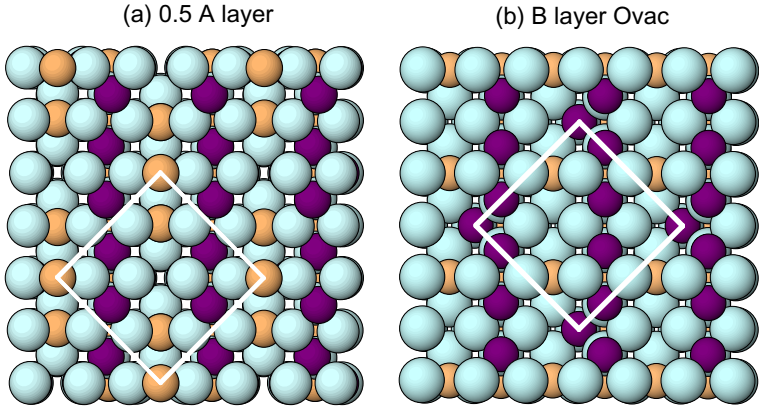

Fig. 2. Top view of (a) the half filled A layer and (b) the B layer with oxygen vacancies above an octahedral iron.

tural determination of the $Fe_3O_4(0\,0\,1)$-surface. The atomic relaxations obtained from DFT calculations and the LEED analysis are compared and discussed in the last section.

2. LEED $I(V)$-measurements

Systematic LEED measurements and LEED $I(V)$-analyses were carried out on the (1 0 0) surface of a natural and a synthetic magnetite sample. A typical LEED-pattern showing the $(\sqrt{2}\times\sqrt{2})R45^\circ$-reconstruction with integer order and superstructure spots is displayed in Fig. 3. In this section we investigate the influence of the preparation conditions on the LEED $I(V)$-curves.

The surfaces of a natural and a synthetic single crystal were prepared by Ar^+ ion sputtering in ultra high vacuum (UHV) and subsequent annealing at 900–1000 K in UHV, $p_{O_2} \leqslant 10^{-10}$ mbar. The degree of cleanliness of the natural sample was checked by X-ray fluorescence analysis, indicating a Mn impurity concentration of 0.2 ppm, obviously too low to influence the surface reconstruction. LEED measurements were performed at 200 K and 300 K on the natural and synthetic sample, respectively. As shown in Fig. 4, the difference between the LEED $I(V)$-curves of the two samples is insignificant; the R-factor between the two sets of experimental curves is $R_P = 0.1$. We assign the deviations between the $I(V)$-curves to the temperature difference mentioned above and to experimental errors. Thus from the LEED point of view the natural and the synthetic sample cannot be distinguished. To explore the influence of the oxygen partial pressure on the $I(V)$-curves, LEED measurements were performed on samples annealed either in UHV ($p_{O_2} = 10^{-10}$ mbar) or in an O_2 atmosphere ($p_{O_2} = 10^{-6}$ mbar). In these experiments the temperature was kept at 80 K to enhance the LEED sensitivity to structural details. The $I(V)$-curves obtained in UHV and in an oxygen atmosphere shown in Fig. 5 agree within a R-factor of $R_P = 0.09$, indicating that the formation of the $(\sqrt{2}\times\sqrt{2})R45^\circ$ superstructure is insensitive to the preparation conditions. The very small curve differences visible in the figure are considered as due to different oxygen defect concentrations of the samples and/or to technical errors, e.g. the alignment of the sample with respect to the electron beam.

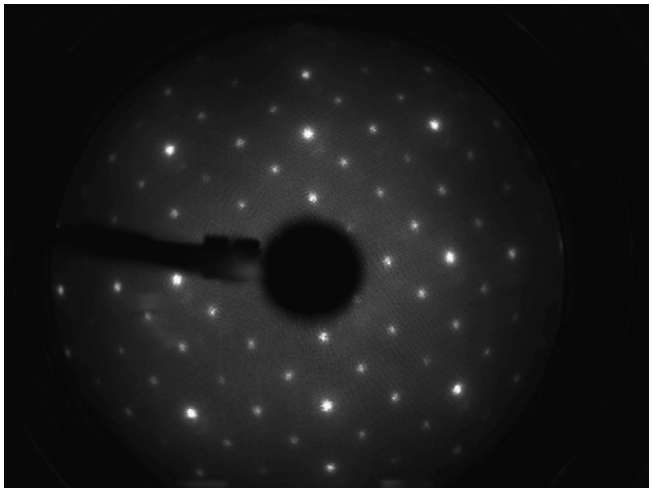

Fig. 3. LEED pattern of $Fe_3O_4(0\,0\,1)$ $(\sqrt{2}\times\sqrt{2})R45^\circ$ at 132 eV.

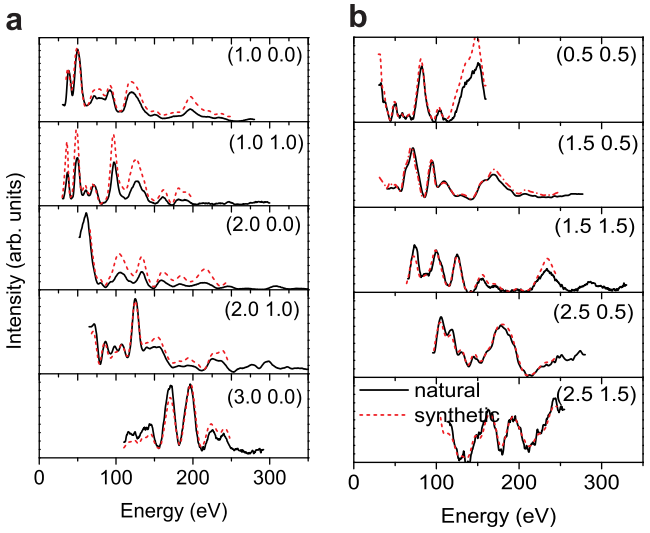

Fig. 4. LEED $I(V)$-curves of the integer order and superstructure reflections of a natural (black) and synthetic (red dotted line) sample, taken at 200 K and 300 K, respectively. (For interpretation of the references in color in this figure legend, the reader is referred to the web version of this article.)

Bulk magnetite undergoes a structural transition at $T_V \sim 122$ K from the cubic phase (space group $Fd3m$) to a monoclinic phase (space group Cc or $P2/c$ [20]). The symmetry of the low temperature phase is still under debate

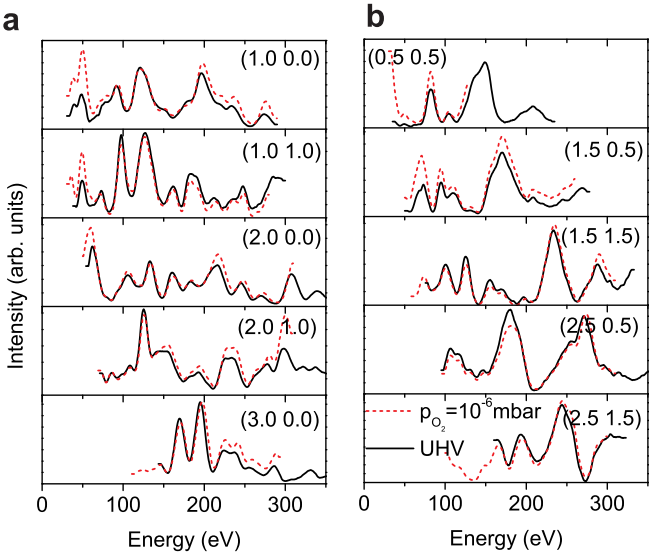

Fig. 5. LEED $I(V)$-curves of the integer order and superstructure reflections of a natural sample annealed in UHV (black) and in oxygen atmosphere at $p_{O_2} = 5\times10^{-6}$ mbar (red dotted line). The LEED measurement was performed at 80 K. (For interpretation of the references in color in this figure legend, the reader is referred to the web version of this article.)

and considered to deviate from the *Pcma* pseudosymmetry by very small atomic displacements [20]. The Verwey transition is accompanied by a drop in conductivity by two orders of magnitude in the low temperature phase [21]. To study the effect of temperature on the sample, we recorded LEED $I(V)$-curves at 80 K and 200 K as shown in Fig. 6. The temperature was measured with a thermocouple attached to a specimen holder provided with a cooling facility. To fix the temperature at 80 K, the sample was first cooled to about 50 K and subsequently heated to 80 K. Surface charging was observed at 50 K but none at 80 K. In the LEED pattern no additional superstructure spots indicative of a phase transition were detected at 80 K. The LEED $I(V)$-curves are quite similar with the main maxima of the $I(V)$-curves occurring at the same energy for both temperatures. The attenuation of intensity with increasing energy in the measurement at 200 K can be explained by thermal motion and/or static displacements around defects. Hence there was no sign of a structural transition between 80 K and 200 K. Our finding can have several explanations: (i) the phase transition does not take place at the surface, (ii) it occurs at a lower temperature, or (iii) it is suppressed by defects or impurities. A transition below 80 K is plausible as has been reported recently for thin films [22]. Recent soft X-ray photoemission measurements found no discontinuous phase transition on well ordered surfaces after surface preparation [23], consistent with our measurements. In order to enhance the sensitivity at high energies, LEED measurements at 80 K and annealing in $p_{O_2} = 10^{-6}$ mbar were used for our structural analysis.

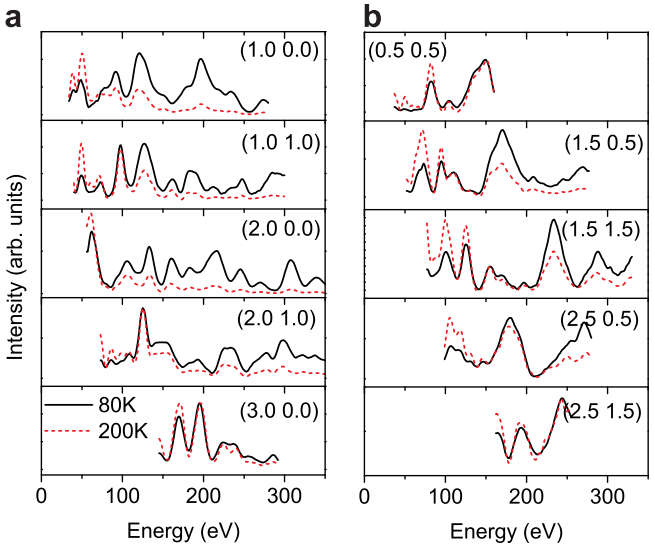

Fig. 6. LEED $I(V)$-curves of the ground structure and superstructure reflections of a natural sample annealed in UHV measured at 80 K, below the Verwey transition (black solid) and 200 K, above the Verwey transition (red dotted line), respectively. Only the overlapping energy range of the two measurements is shown and the two curves are scaled to fit at medium energies for better comparison. (For interpretation of the references in color in this figure legend, the reader is referred to the web version of this article.)

3. Influence of the phase shifts in the LEED analysis: conventional vs. DFT-derived

In LEED $I(V)$-analyses from ionic crystals the level of agreement between experimental and calculated $I(V)$-curves is often found considerably worse than what is achievable for clean metal surfaces. Besides the structural complexity of oxide surfaces, one reason lies in the calculation of the muffin-tin (MT) potential of ionic crystals. The phase shifts used for LEED $I(V)$-calculations are usually obtained from a superposition of atomic potentials, ionicity is neglected in most cases. The Madelung potential is often used to calculate the lattice energy of ionic compounds but does not allow to derive the electron density inside the MT-sphere. Therefore, the introduction of a Madelung potential and the use of ionic radii is not appropriate for the construction of the muffin-tin potential. Our initial LEED analysis used a superposition of potentials from neutral atoms in combination with optimized MT radii [19]. This approach was recently applied to determine the surface structure of $Ca_{1.5}Sr_{0.5}CuO_4(001)$ [24]. We note that the phase shifts and LEED intensities are sensitive to the MT radii; noticeable differences occur when the MT of the oxygen atom is increased by 0.05 Å. This scheme of optimization of MT radii generates a crystal potential consisting of spherical MT potentials joined continuously to a constant interstitial potential. The continuity ensures that electron scattering resonances due to accidental standing waves in the MT spheres are reduced to a minimum; remaining resonances caused by a discontinuous potential gradient at the MT radius are negligible. The MT radii depend on the number, species, and distances of neighbors and were determined to be 0.92 and 0.96 Å for Fe and O, respectively.

A purpose of the present paper is to exploit DFT derived potentials for calculating electron scattering phase shifts for ions in crystals. Like in an earlier work on magnetite [15], we used the WIEN2k implementation of DFT [25] within the generalized gradient approximation (GGA) [26]. Characteristic of the method is the separation of space in non-overlapping MT spheres around the atomic positions and interstitial region. In the present work only the DFT potential within the MT spheres was used for generating phase shifts. DFT calculations both for the bulk and the (100) surface of magnetite were used, but no substantial difference in the phase shifts was found for atoms lying near the surface. We attribute this to the relatively small muffin tin radii that had to be used for the surface DFT-calculation due to the strong relaxation in the surface layers.

The phase shifts obtained from the superposition scheme and from DFT calculations are compared in Fig. 7, and the differences are found to be marginal. Both sets of phase shifts were applied in the final least-squares LEED optimization. The corresponding calculated and experimental $I(V)$-curves are displayed in Fig. 8 and show an equally good agreement with the measured ones. In a re-

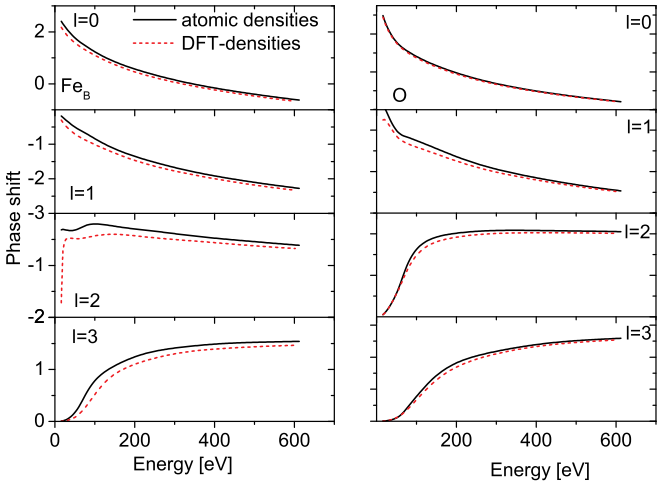

Fig. 7. Phase shifts of octahedral iron (left) and oxygen (right) obtained from a superposition of atomic potentials (black) and from the DFT-calculation for bulk Fe_3O_4 (red line). (For interpretation of the references in color in this figure legend, the reader is referred to the web version of this article.)

cent LEED analysis of the TiO_2(1 1 0) surface Lindsay et al. [27] replaced electron scattering phase shifts produced by an atomic superposition scheme [28] by ones generated from DFT electron densities [29], thereby bringing down the *R*-factor from 0.64 to 0.29. Unlike the reported dramatic change in the *R*-factor with phase shift design, our *I*(*V*)-curves and structural results agree excellently with both generation methods. The corresponding *R*-factors are 0.33 and 0.34 for the phase shifts derived from the DFT-calculation and the superposition scheme, respectively.

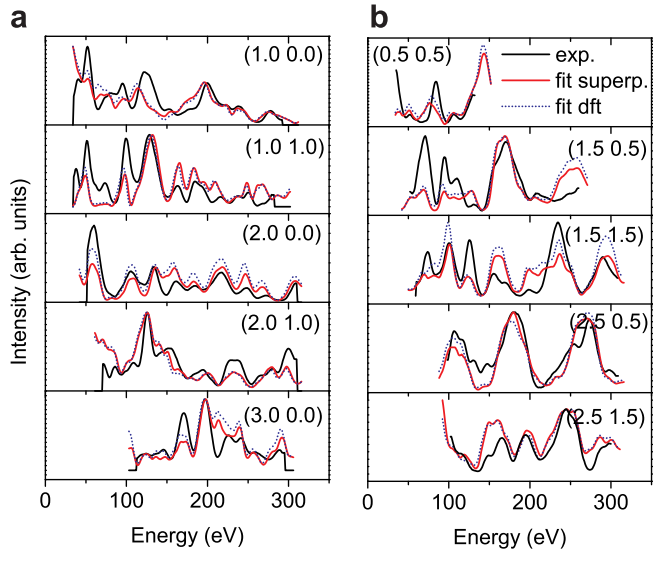

Fig. 8. Best fit LEED *I*(*V*)-curves. The experimental data of the natural sample at 80 K is represented by a thick black solid line, the calculated intensities using the superposition scheme with optimized MTs ($R = 0.34$) and DFT derived ($R = 0.33$) phase shifts are marked by a red solid and blue dotted line, respectively. Structural parameters are given in Table 2. (For interpretation of the references in color in this figure legend, the reader is referred to the web version of this article.)

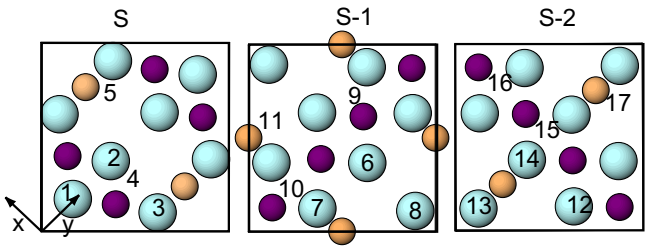

Fig. 9. Top view of the surface (S) and the subsequent subsurface layers (S-1) and (S-2) where the positions of the atoms displayed in Table 2 are marked. Large circles denote oxygen, small orange (light grey) and purple (dark grey) spheres denote tetrahedral and octahedral iron. (For interpretation of the references in color in this figure legend, the reader is referred to the web version of this article.)

4. Structural refinement combining DFT and LEED

A quantitative LEED analysis was performed for a variety of surface terminations, including the B layer termination, a half-filled A layer with Fe_A either above the B layer or nearly coplanar in the B layer (see Fig. 2a), as well as B terminations with oxygen vacancies above a Fe_B ion (see Fig. 2b) or next to a subsurface Fe_A. The experimental *I*(*V*)-curves of the natural sample annealed in an oxygen atmosphere and measured at 80 K were used in the structural optimization. In the initial search the two outermost BA layers of each model were refined; ten phase shifts were used together with isotropic temperature factors corresponding to bulk Debye-temperatures of 400, 320 and 650 K for Fe_B, Fe_A, and oxygen, respectively. The *R*-factors for the optimized models are shown in Table 1. The results clearly indicate a preference for the B layer termination, all other models produce significantly higher *R*-factors.

The experimental and best-fit *I*(*V*)-curves for the modified B layer are shown in Fig. 8. The *R*-factor obtained after further refinement with 53 free parameters and isotropic temperature factors was $R_P = 0.38$, and the inclusion of anisotropic thermal vibrations [31] led to a further drop to $R_P = 0.34$. This value is relatively high but in line with the ones obtained for other oxide surfaces, e.g. $R_P = 0.29$ for TiO_2 (1 1 0) [27] and $R_P = 0.28$ for $Ca_{1.5}Sr_{0.5}RuO_4$ (0 0 1) [24]. Besides the already discussed influence of the phase shifts, the relatively low level of agreement between

Table 1
R-factors for the optimized models

Model	R_P
Modified B layer (Fig. 10)	0.34
Half occupied A layer (Fig. 2a)	0.60
B layer with O-vacancy above Fe_B (Fig. 2b)	0.65
B layer with O-vacancy next to Fe_A	0.66

Pendry's *R*-factor has been used [30].

Table 2
Atomic displacements in x, y and z-direction and total (Δr) with respect to the bulk coordinates obtained from the DFT-optimization

	Δx (Å)	Δy (Å)	Δz (Å)	Δr (Å)
B layer(S)				
O1	0.00 (0.00)	0.36 (0.55)	0.02 (0.25)	0.36 (0.60)
O2	0.00 (0.00)	−0.14 (0.00)	0.11 (0.24)	0.18 (0.24)
O3	−0.06 (−0.12)	−0.17 (−0.09)	0.09 (0.01)	0.20 (0.15)
Fe_B4	−0.04 (−0.03)	0.13 (0.19)	0.14 (0.22)	0.19 (0.29)
Fe_A5	0.08 (0.18)	0.02 (0.00)	−0.10 (−0.19)	0.13 (0.26)
B layer(S-1)				
O6	0.00 (0.04)	0.02 (0.00)	0.12 (−0.03)	0.12 (0.05)
O7	0.09 (0.09)	−0.01 (0.00)	−0.06 (−0.04)	0.11 (0.10)
O8	−0.01 (0.05)	−0.04 (0.29)	0.12 (0.18)	0.13 (0.34)
Fe_B9	0.00 (0.00)	0.05 (0.08)	−0.05 (−0.06)	0.07 (0.10)
Fe_B10	0.00 (0.00)	−0.09 (0.05)	−0.01 (0.18)	0.09 (0.19)
Fe_A11	0.00 (0.00)	0.00 (0.00)	0.05 (0.16)	0.05 (0.16)
B layer(S-2)				
O12	Fix (0.01)	Fix (0.16)	Fix (−0.10)	Fix (0.18)
O13	Fix (0.00)	Fix (−0.06)	Fix (0.00)	Fix (0.06)
O14	Fix (0.00)	Fix (0.06)	Fix (0.02)	Fix (0.07)
Fe_B15	Fix (0.00)	Fix (0.00)	Fix (0.18)	Fix (0.18)
Fe_B16	Fix (0.07)	Fix (0.00)	Fix (−0.06)	Fix (0.10)
Fe_A17	Fix (0.00)	Fix (−0.13)	Fix (−0.11)	Fix (0.17)

The corresponding values from the LEED-analysis are given in brackets. The numbering of the atoms and the coordinate system corresponds to Fig. 9.

measured and fitted $I(V)$ curves for oxide surfaces can be attributed to surface roughness, domain boundaries and the presence of defects (e.g. oxygen vacancies) in the samples.

A common problem when using a single optimization technique is that the structural refinement may be trapped in a local minimum. To avoid this, we applied a combined optimization approach for determining the structure of Fe_3O_4 (001), starting the LEED analysis from the DFT geometry of Ref. [15]. Subsequently, we performed a further DFT optimization, taking the LEED coordinates as an input. We note that in the DFT calculation only the coordinates of the top two BA layers were relaxed due to the high numerical demand, while the LEED analysis included three BA units. Atomic positions below the third B layer were kept fixed. In total 43 parameters[1] were optimized in the DFT calculation and 53 in the LEED analysis. The shifts of the atoms with respect to the ideal bulk positions are shown in Table 2.

The main feature of the surface reconstruction of Fe_3O_4 (001) is that substantial relaxations occur perpendicular to the B rows in the surface layer. In particular, for surface oxygen O1 (the oxygen atom without subsurface tetrahedral neighbor) we found a displacement in y-direction of 0.36 Å from DFT and 0.55 Å from LEED, and for the surface octahedral iron FeB4 we obtained a lateral shift of 0.13 Å from DFT and 0.19 Å from LEED. These distortions of FeB perpendicular to the [1 1 0]-direction give rise to a transversal *wave* along [1 1 0] with neighboring rows going in antiphase to each other and thus forming the $(\sqrt{2}\times\sqrt{2})R45^\circ$-reconstruction shown in Fig. 10. Such a *wave-like* pattern is also observed in STM-measurements [11,18]. In the z-direction, the atoms in the surface layer relax inwards, while the subsurface A and B layers relax outwards.

Through repeated cycles of DFT and LEED refinement we could obtain a good overall agreement between the two methods both with respect to size and direction of the relaxations. In particular, some atomic displacements were slightly enhanced with respect to the initial DFT optimization reported in [15], e.g. the lateral shift of O1 and FeB4 was 0.30 Å and 0.09 Å in the initial and 0.36 Å and 0.13 Å in the final DFT-structure, respectively. In general, we obtain stronger relaxations especially for the oxygen positions from LEED than from DFT. One reason is that the LEED optimization involves more layers than the DFT leading to stronger relaxations in the z-coordinate (e.g. O1 and O7). On the other hand, LEED is less sensitive to the oxygen positions, for example above 100 eV the total scattering cross section of oxygen is about one third of that of iron. Changes of the lateral position of O1 of up to 0.2 Å did not influence significantly the R-factor. This indicates a rather flat and broad minimum of the R-factor and is possibly related to the large thermal vibrations. Similarly, a flat and broad minimum of the potential energy with respect to the oxygen coordinate was obtained from DFT for TiO_2(1 1 0) [32]. Finally, the uncertainty in the positions determined with LEED increases in deeper layers. The measurements are also likely to be influenced by defects in the sample, e.g. by oxygen vacancies; however, such structural features are not included in the present DFT and LEED models.

5. Summary

Our LEED measurements show no noticeable differences between the natural and the synthetic sample. In agreement with the surface phase diagram obtained in the framework of *ab initio* thermodynamics [15], there was no significant dependence on oxygen partial pressure during sample preparation. We used the DFT and LEED methods self-consistently for determining the structure of Fe_3O_4(0 0 1), and we claim that such a combination of approaches is necessary for achieving a quantitative agreement between these surface analysis techniques and for ensuring a global minimization. The LEED and the previous XRD results indicate that relaxations may reach deeper than three BA layers.

The validity of the DFT model for the surface termination of Fe_3O_4(0 0 1) [15] is confirmed by the present LEED $I(V)$-analysis in accord with earlier results obtained by XRD [15] and STM [11,18]. Our results show that the Fe_3O_4(1 0 0) surface is terminated by a B layer, a structure previously discarded on the basis of electrostatic argu-

[1] The number of parameters optimized in the DFT-calculation is higher because a lower symmetry was used (one of the mirror planes was not explicitely taken into account).

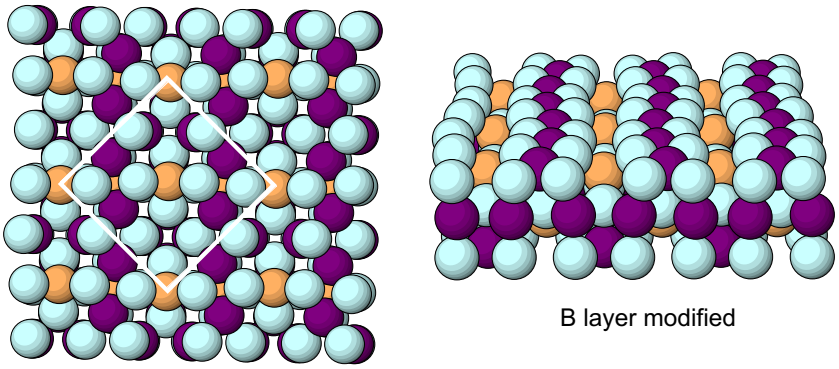

Fig. 10. Top and side view of the final DFT/LEED structure of the modified B layer.

ments. The stabilization of the surface involves a Jahn–Teller distortion with a *wavelike* displacement of iron and oxygen atoms in the top B layer, whereby a $(\sqrt{2}\times\sqrt{2})R45^\circ$ superstructure is formed.

Acknowledgement

This work is supported by the DFG, PE 883/1-1. We acknowledge the Grant of computational time at the Leibniz Rechenzentrum.

References

[1] A. Yanase, K. Siratori, J. Phys. Soc. Jpn. 52 (1984) 312.
[2] Z. Zhang, S. Satpathy, Phys. Rev. B 44 (1991) 13319.
[3] P.W. Tasker, J. Phys. C 12 (1979) 4977.
[4] J.P. LaFemina, Crit. Rev. Surf. Chem. 3 (1994) 297.
[5] J.M. Gaines et al., Surf. Sci. 373 (1997) 85.
[6] G. Tarrach et al., Surf. Sci. 285 (1993) 1.
[7] S.A. Chambers, S. Thevuthasan, S.A. Joyce, Surf. Sci. 450 (2000) L273.
[8] A.V. Mijiritskii, D.O. Boerma, Surf. Sci. 486 (2001) 73.
[9] F.C. Voogt et al., Phys. Rev. B 60 (1999) 11193.
[10] J.R. Rustad, E. Wasserman, A.R. Felmy, Surf. Sci. 432 (1999) L583.
[11] B. Stanka et al., Surf. Sci. 448 (2000) 49.
[12] G. Mariotto, S. Murphy, I.V. Shvets, Phys. Rev. B 66 (2002) 245426.
[13] I.V. Shvets, G. Mariotto, K. Jordan, N. Berdunov, R. Kantor, S. Murphy, Phys. Rev. B 70 (2004) 155406.
[14] N. Spiridis, J. Barbasz, Z. Lodziana, J. Korecki, Phys. Rev. B 74 (2006) 155423.
[15] R. Pentcheva, F. Wendler, H.L. Meyerheim, W. Moritz, N. Jedrecy, M. Scheffler, Phys. Rev. Lett. 94 (2005) 126101.
[16] C.M. Weinert, M. Scheffler, in: Defects in Semiconductors, H.J. Bardeleben (Ed.), Mat. Sci. Forum 25 (1986) 10–12.
[17] K. Reuter, M. Scheffler, Phys. Rev. B 65 (2002) 035406.
[18] M. Fonin, R. Pentcheva, Yu.S. Dedkov, M. Sperrlich, D.V. Vyalikh, M. Scheffler, U. Rüdiger, G. Güntherodt, Phys. Rev. B 72 (2005) 104436.
[19] J. Rundgren, Phys. Rev B 68 (2003) 125405.
[20] J.P. Wright, J.P. Attfield, P.G. Radaelli, Phys. Rev. B 66 (2002) 214422.
[21] E.J.W. Verwey, Nature (London) 144 (1939) 327.
[22] Chih-Huang Lai, Po-Hsiang Huang, Yu-Jen Wang, R.T. Huang, J. Appl. Phys. 95 (2004) 7222.
[23] D. Schrupp, M. Sing, M. Tsunekawa, H. Fujiwara, S. Kasai, A. Sekiyama, S. Suga, T. Muro, V.A.M. Brabers, R. Claessen, Europhys. Lett. 70 (2005) 789.
[24] V.B. Nascimento, R.G. Moore, J. Rundgren, Jiandi Zhang, Lei Cai, R. Jin, D.G. Mandrus, E.W. Plummer, Phys. Rev. B 75 (2007) 035408.
[25] P. Blaha, K. Schwarz, G.K.H. Madsen, D. Kvasnicka, J. Luitz, WIEN2k, An Augmented Plane Wave + Local Orbitals Program for Calculating Crystal Properties, Karlheinz Schwarz, Techn. Univ. Wien, Austria, 2001, ISBN 3-9501031-1-2.
[26] J.P. Perdew, K. Burke, M. Ernzerhof, Phys. Rev. Lett. 77 (1996) 3865.
[27] R. Lindsay, A. Wander, A. Ernst, B. Montanari, G. Thornton, N.M. Harrison, Phys. Rev. Lett. 94 (2005) 246102.
[28] DLPHASE computer program package available from <http://www.ccp3.ac,uk>.
[29] V.R. Saunders, R. Dovesi, C. Roetti, R. Orlando, C.M. Zicovich-Wilson, N.M. Harrison, K. Doll, B. Civalleri, I. Bush, Ph. D'Arco, M. Llunell, CRYSTAL 2003 User's Manual, University of Turin, Turin, 2003.
[30] J.B. Pendry, J. Phys. C: Solid State Phys. 13 (1980) 937.
[31] W. Moritz, J. Landskron, Thermal vibrations at surfaces analysed with LEED, in: W. Schattke, M.A. Van Hove (Eds.), Solid-State Photoemission and Related Methods, Wiley-VCH, 2003, pp. 433–459.
[32] N.M. Harrison, X.-G. Wang, J. Muskat, M. Scheffler, Faraday Discuss. 114 (1999) 305.